# Non-conventional Structural Patterns for Tall Buildings: from Diagrid to Hexagrid and Beyond

Elena Mele *, Massimiliano Fraldi, Gian Maria Montuori, and Gianpaolo Perrella
elenmele@unina.it, fraldi@unina.it, giovannimaria.montuori@unina.it
Department of Structures for Engineering and Architecture, University of Naples Federico II, Italy

**Abstract:** In this paper, a first insight on "non-conventional" structural patterns, to be adopted in tube configurations for tall buildings, is provided. The idea is to investigate the mechanical properties of non conventional structural patterns, both regular (Hexagonal Grid, i.e. HexaGrid) and irregular (grid inspired by the Voronoi tessellation), in order to assess their applicability, and to compare their potential efficiency to the more popular diagrid system. For this purpose, a classical homogenization-based micromechanical approach has been employed, by deriving sensitivity analyses and generalized stress-strain relationships for both regular and geometrically distorted irregular pattern units, the latter obtained by perturbing prescribed key geometrical features of the Representative Volume Element to control Voronoi morphologies and predict associated mechanical properties. On the basis of a simple stiffness criterion, a preliminary design procedure is proposed and applied to a tall building case study whose bearing skeleton is conceived on the basis of the investigated unconventional structural patterns.

**Keywords:** Voronoi, Hexagrid, Steel Structure, Homogenization Method, Stiffness Design.

## Introduction

The fundamental conceptual simplification for the structural design of tall buildings, "The Idea" (Baker 2013), is to consider the building as a giant cantilever beam, with overturning moment and shear force known a priori, and lateral deformation given by a combination of flexural and shear modes, i.e.:

$$\delta_{tot} = \delta_{bending} + \delta_{shear} = \frac{q H^4}{8 EI} + \frac{q H^2}{2 GA} \chi \qquad (1)$$

where: $q$ is the uniform horizontal load representative of the wind action, H is the beam length (i.e. the building height), A and I are respectively the area and the moment of inertia of the beam cross section, E and G are respectively the axial and shear moduli and $\chi$ is the shear factor. A stiffness based criterion for preliminary sizing the cross section (area and inertia) of the equivalent beam consists in setting a maximum value for the top displacement, e.g.:

$$\delta_{max} = \frac{H}{500} = \delta_{tot} \qquad (2)$$

The ideal cross section for a cantilever beam is a hollow section; structural configurations for tall buildings best reflecting this optimum section shape of the equivalent giant beam are the ones employing the tube concept: the four building facades act as two flanges and two webs of the hollow cross section, the former mainly resisting bending moment through axial tension and compression, the latter providing shear resistance.

It should be pointed out that the building facades are usually made of a grid of structural members instead of solid panels, and the shear-resisting mechanism of the façade grid strongly affects the tube efficiency. In this perspective, diagrid structures - the latest mutation of tube structures - show an extraordinary efficiency, related to the adopted geometrical pattern: thanks to the triangle tessellation of the façades, internal axial forces are largely prevalent in the structural members, thus shear lag effects and racking deformations are minimized (Mele *et al.* 2014). Being also adaptable to whatever surface, diagrid is becoming the most used structural solution for tall buildings of complex form (Montuori *et al.* 2013, 2014 a, 2014b).

However, alternative, non conventional, geometrical patterns are worth of consideration for their structural and aesthetical qualities. Natural patterns, i.e. geometrical patterns observable in nature which reflect the unquestionable laws of economy and efficiency (Perez and Gomez 2009; Hensel *et al.* 2009), can be a fruitful and almost endless source of inspirations for efficient man-made structures, at all scale levels (from the very tiny - material design - to the biggest – tall buildings - embracing all intermediate steps). In the context of material science and engineering, heterogeneous and cellular materials, as well as hierarchical natural organisms, have been intensely studied in the last decades (Gibson and Ashby 1988; Fraldi and Cowin 2004; Lakes 1993) and inspired the biomimicry

approach for the conception and fabrication of man made products. An example is the adoption of the hexagon-based beehive configurations for creating honeycomb structure which provides a composite material with minimal density and relative high compression and shear properties, thereby obtaining high efficiency (strength - or stiffness - to weight ratio).

The lesson of the nature has been received in different ways and at different extents by the engineering design disciplines: while composite materials, foam structures, sandwich panels are typical applications at the material-scale level, a more superficial and incomplete awareness of the efficiency philosophy taught by nature can be found at macro-scale level, in the field of civil engineering. In particular, the structural designers operating in the field of building engineering is less prone to explore ideas coming from the field of natural structures and to experiment novel bio-inspired structural systems.

**Figure 1**. Example of non conventional structural patterns

Actually, some suggestions in this direction come from the architecture realm, with a stunning variety of proposals, projects, visions, more or less consciously inspired by natural structures, such as foams, seashells, radiolariae, glass sponge, bone tissue, coral or cactus skeletons, etc. It is worth noticing that the above patterns are often based on non regular hexagonal meshes, that can be represented by Voronoi diagrams (Voronoi 1908; Montuori *et al.* 2015). In figure 1 a collection of tall buildings inspired by natural patterns is shown, mainly concerning architecture proposals in design competitions.

The design, modelling and analysis of such structural patterns are not as straightforward as in the case of the traditional orthogonal pattern (the beam/column frame), therefore a challenging and exciting task for the research in structural engineering is the attempt to bridge the gap between design visions and actual constructability.

In this perspective, the authors have undertaken a wide research activity starting from the idea that natural structures, as well as cross-fertilization between science and engineering, can inspire also man-made products at the mega level, namely structures for high-rise and long-span buildings, thus providing a radically new repertoire of forms and systems for challenging architectures. As a first step of the research undertaken by the authors, hexagon-based patterns are currently being examined as tube structural grids for tall buildings. Objects of the study are both regular and non-regular (Voronoi-like) patterns: the formers are patterns made by uniform tessellation of hexagonal cells, appointed as hexagrids, while the latters, the non regular patterns, are either fully based on Voronoi diagrams, or mixed regular (hexagrids) and irregular (Voronoi) patterns.

In the paper (Montuori et al. 2015) the authors have focused attention to regular horizontal hexagrid patterns (i.e. hexagonal patterns made only by horizontal and diagonal structural members). Major aims of the paper have been the investigation of the structural properties of hexagrids, the assessment of their applicability in tall buildings, the definition of a simple design procedure for the preliminary sizing of the structural members composing the hexagonal pattern, and the comparison of their potential efficiency to the more popular diagrid systems.

In this paper, non regular patterns based on Voronoi diagrams are considered for structural grid of tall building façades, thus obtaining Voronoi tube structures. In section 2 the objective and approach utilized in the paper are stated; then in section 3, the geometrical definition of Voronoi diagram is introduced, and the procedure for the generation of Voronoi diagrams adopted in this paper is explained; in section 4 and 5 the general methodology for the mechanical characterization and the homogenization process of a structural grid is presented and applied to regular hexagrid; then in section 6 and 7 the additional steps required for a non-regular, Voronoi-like grid are provided and discussed; finally in section 7 a design procedure is proposed, applied to and validated for a model building.

## Objective of the work and methodology

With reference to the stiffness based design criterion expressed through Eqs. (1-2), an appropriate procedure for taking into account the discrete nature of the structural grid acting as flanges and webs of beam cross section should be defined in order to preserve the conceptual scheme of equivalent cantilever beam; in other words, in the Eq. (1) appropriate values $(EI)_{grid}$ and $(GA)_{grid}$ should be substituted to EI and GA:

$$\delta_{tot} = \delta_{bending} + \delta_{shear} = \frac{q H^4}{8(EI)_{grid}} + \frac{q H^2}{2(GA)_{grid}} \chi \qquad (3)$$

This kind of approach is proposed by (Kwan 1994), with a methodology for dealing with frame tube panels as equivalent orthotropic membranes, so that the framed tube could be analyzed as a continuous structure.

A more general methodology is proposed in this paper for dealing with grid-like structures: the idea is to model whichever grid as a continuous depleted medium, characterized by penalized mechanical properties, according to the classical micromechanical approach based on homogenization methods (Hashin and Shtrikman 1996); the macroscopic penalized properties of the structure, appointed as effective properties, will account for both the mechanical properties of the solid matrix and the micro-structural features of the grid, namely topology, density, orientation.

Basically, the procedure consists in evaluating the effective axial and shear moduli of the grid, which account for the geometric and elastic properties of structural members as well as for the geometrical pattern of the grid. Once the effective axial stiffness and racking shear stiffness of the grid are evaluated, the standard formulae defined for a solid tube can be utilized for calculating the horizontal deflections of the homogenized grid tube Eq. (3); that is, the stiffness based design criterion for a tube tall building, Eq. (2), can be specified substituting EI and GA with $(EI)_{grid}$ and $(GA)_{grid}$, respectively, and the member cross section properties required for satisfying the limit deflection can be obtained.

This is the approach already adopted in (Montuori *et al.* 2015) for regular hexagonal grids, where the mechanical characterization and the consequent homogenization of the grid consists in the assessment of the structural behaviour of a simple, unit cell (the Representative Volume Element, RVE, of the grid), easily identifiable thanks to the grid regularity and periodicity.

In this paper the approach is extended to the case of irregular grids, namely a grid obtained from the Voronoi diagram; in this extension, a first difficulty arises in the identification of the unit cell, which, quite trivially, does not exist due to the non-periodicity and randomness of the grid.

The approach here proposed for overcoming such difficulty consists in defining the correlation between the average mechanical properties of the irregular (Voronoi) patterns and regular (hexagrid) counterparts on a statistical basis; the aim is to define the appropriate correction factors which allow for calculating the average mechanical proprieties of the Voronoi patterns, known the ones of a reference regular pattern.

## Voronoi diagrams: geometry and generation

### Geometric definition

The Voronoi diagram (or tessellation) is the mathematical explanation for a visual pattern often found in nature, as in the structure of leaves, in the skin of animals, and in several life forms. In mathematics, “a Voronoi diagram is the division of a space into contiguous neighbouring cells, which relate to a set of points (Voronoi sites) in that space; each point has an associated cell consisting of all the points closer to that site than any other” (Burry and Burry 2010).

For the construction of the Voronoi diagram, firstly a set of points (appointed as seeds, sites, or generators) should be defined; then, for each seed, a corresponding region (appointed as Voronoi cell) is obtained as the one consisting of all points closer to that seed than to any other. The Voronoi construction can be carried out both in plane, giving rise to two-dimension Voronoi tiling, and in space, giving rise to three-dimension Voronoi tessellations.

Theoretical and practical applications of Voronoi diagrams widely spread over several fields of science and technology, going from astrophysics, epidemiology, geometry, networking, hydrology, meteorology, ecology, computer graphics, computational fluid dynamics, etc (Aurenhammer 1991). In particular, Voronoi tessellations are widely used in the context of material science, for representing polycrystalline microstructures of metallic alloys (Wigner and Seitz 1933), and in the field of biology, for modelling different natural structures, including cells and bone microarchitecture (Bock *et al.* 2010); in the framework of material engineering and design, the Voronoi diagram is the major approach for modelling and analyzing cellular materials and solid foams (Silva and Gibson 1997; Vajjhala *et al.* 2000).

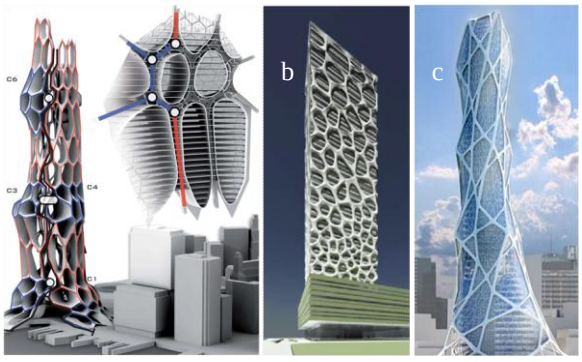


**Figure 2**. Voronoi patterns for tall buildings: Use Arrangement” Christian Hahn eVolo 2010 Skyscraper competition entry; SOM competition entry, tower in Tianjin; Lava Bionic Tower.

The division of space according to Voronoi diagrams and their numerous generalizations are a rich source for the design of spatial structures, which

inspired many architects. The concept works in the plane, for input points on a surface, as well as in space, as can be seen from the skyscraper proposals provided in figure 2a (eVolo 2010), figure 2b (Beghini *et al.* 2014) and figure 2c (LAVA 2017), which explicitly refer to both 3D and 2D Voronoi tessellations; in particular it can be observed that the project represented in figure 2a utilizes the Voronoi partition as a 3D strategy for space subdivision, that can be an interesting conceptual approach for unifying form, function and structure in the building design.

**Voronoi tessellation**

Several methods (Zheng *et al.* 2005; Fazekas *et al.* 2002; Zhu *et al.* 2001; Silva *et al.* 1995) are reported in the scientific literature for the generation of the Voronoi tessellation. The method proposed in (Li *et al*. 2005) is used in the following, since it allows for controlling the irregularity degree of the Voronoi diagram.

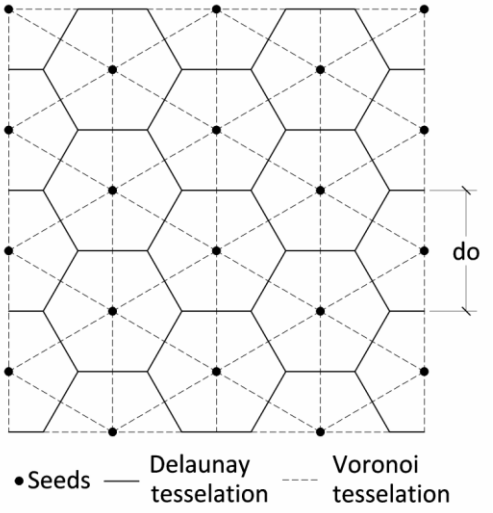


**Figure 3**. Voronoi construction applied to Delaunay disposition of seeds.

The starting point is a regular geometry, obtained by applying the Voronoi construction to a regular grid of seeds; in particular in this paper, regular hexagonal patterns are considered as initial geometries. figure 3 shows how regular honeycomb can be generated from seeds arranged at the vertexes of equilateral triangles (i.e. according to a Delaunay tessellation, which is dual to Voronoi diagram).

The second step is to randomly modify the regular array of seeds; for this aim, the coordinates $\left(\bar{x}_1^s, \bar{x}_2^s\right)$ of the generic seed S are perturbed (figure 4) through two random variables $\vartheta_s \in [0, 2\pi]$ and $\varphi_s \in [-1, 1]$. The variable $\vartheta_s$ is a random angle between the $x_1$ axis and the line connecting the perturbed and the non perturbed position of the seed s; it is assumed to be distributed according to a uniform distribution with the following probability density function:

$$P_\vartheta(\vartheta_s)=\begin{cases}1/2\pi & 0 \le \vartheta_s \le 2\pi \\ 0 & \vartheta_s < -1,\ \vartheta_s > 1\end{cases} \qquad (4)$$

The variable $\varphi_s$ is a random scale factor, distributed according to a uniform distribution with the following probability density function:

$$P_\varphi(\varphi_s)=\begin{cases}1/2 & -1 \le \varphi_s \le 1 \\ 0 & \varphi_s < -1,\ \varphi_s > 1\end{cases} \qquad (5)$$

Therefore the perturbed coordinates $(x_1^s, x_2^s)$ are defined by using the following equations

$$x_1^s = \bar{x}_1^s + \alpha\left(d_0 \operatorname{Cos}\vartheta_s\right)\cdot\varphi_s \qquad (6)$$

$$x_2^s = \bar{x}_2^s + \alpha\left(d_0 \operatorname{Sin}\vartheta_s\right)\cdot\varphi_s \qquad (7)$$

where $\alpha \in [0,1]$ defines the irregularity degree of the Voronoi grid, namely $\alpha = 0$ corresponds to the regular hexagonal grid, while $\alpha = 1$ corresponds to Voronoi grid with maximum degree of irregularity.

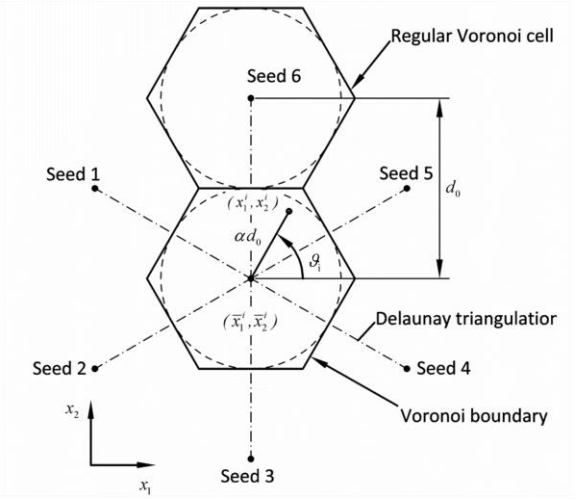


**Figure 4**. Geometric perturbation of the coordinates of regular array of seeds.

The last step is to apply the Voronoi tessellation to the arrays of points modified through the equations (6) and (7), in order to obtain patterns with irregularity governed by the α parameter. The fundamental role played by α is clearly shown in figure 5, which provides three specimens with the same overall dimensions and number of unit cells but with different degree of irregularity, i.e. different values of α adopted in the generation process. For $\alpha = 0$ (figure5a) a regular honeycomb structure is generated; increasing α (figure5b), the irregularity of the pattern increases and for $\alpha = 1$ (figure 5c) a geometry with the maximum irregularity degree is obtained. Of course, for each values of α (i.e. for each level of irregularity), infinite geometric configurations can be generated varying the random parameters $\varphi_s$ and $\vartheta_s$.

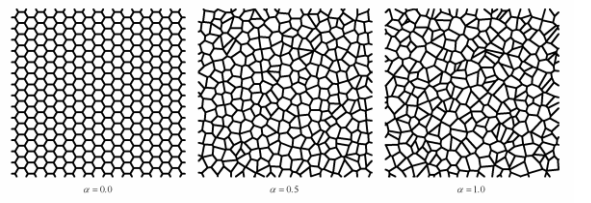


**Figure 5**. Effect of α: a) α = 0; b) α = 0.5; c) α = 1.

The process described to generate the Voronoi geometries has been automated by implementing a specific algorithm in Grasshopper environment (Rhinoceros 3D®). The algorithm is made by a cluster of functions which allows to: i) create a regular arrangement of seeds (as shown in figure 3); ii) set the required irregularity level; iii) alter the coordinates of the s-th seed by means of the Eqs. (6-7), using two different random engines for the two random variables, $\varphi_s$ and $\vartheta_s$; iv) generate the Voronoi geometry, i.e. the polygonal cells, from the perturbed seeds. Using this algorithm, a large number of samples can be generated with a rigorous method and with low time consumption.

## Mechanical approach for regular and irregular patterns

In order to apply the design procedure described in the previous section, the correlation between the geometrical characteristics of the irregular Voronoi patterns and the mechanical properties of the homogenized material should be identified. The idea is to use the typical approach in the field of cellular materials, in which the mechanical properties of a real cellular solid are calculated defining an ideal unit cell (i.e. the geometric unity that through replication allows to obtain the overall geometric pattern without overlaps or gaps). For examples, hexagonal cell are used to describe many 2D honeycomb-like cellular solids, while cubic, tetrahedral and dodecahedral solid are used for tridimensional cellular materials. Using this simplified unit cells, the relationships between the microstructure and the overall mechanical proprieties (e.g. relative density, axial and shear stiffness) can be derived in closed form (Silva *et al.* 1995; Gibson and Ashby 1997; Li *et al*. 2003). As already recalled, a similar approach, though applied to a rectangular orthogonal pattern, was used in (Kwan 1994) for the design of framed tube structures, and more recently in (deMeijer 2012) and (Montuori *et al*. 2015) for the design and analysis of hexagrid and diagrid structures.

In the following a brief description of the overall mechanical proprieties useful for the design process, is reported.

The overall mechanical response can be obtained starting from the unit cell as well; in particular it is necessary to introduce the so-called Representative Volume Element (RVE), which is defined as the smallest homogeneous material volume which macroscopic constitutive relationships must be referred to (Nemat-Nasser and Hori 1999); therefore the RVE can be considered as the structural idealization of the unit cell.

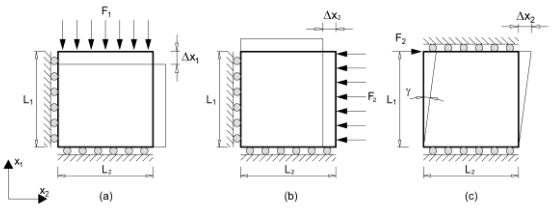


**Figure 6**. RVE mechanical tests: a) axial test along $x_1$; b) shear test.

Once defined the RVE, the effective mechanical properties of the 2D structural grid, $E_1^*$, $E_2^*$, $G_{12}^*$ and $G_{21}^*$ can be obtained by means of numerical tests on the RVE; in particular, the Elastic Axial Modulus $E_1^*$ is defined as the ratio of the uniaxial normal stress $\sigma_1$ divided by the uniaxial strain $\varepsilon_1$ in the elastic range, for the reference specimen (the RVE) subject to simple axial load, as illustrated in figure 6a for the direction of load $x_1$, as well as in figure 6b, for the direction of load $x_2$. Normal stress is the average normal force ($F_1$) acting perpendicularly on a surface per unit cross-sectional area ($L_2 \cdot b$). Strain is the shortening, or lengthening ($\Delta x_1$) of the RVE divided by the initial length ($L_1$) in the loaded direction.

$$E_1^* = \frac{\sigma_1}{\varepsilon_1} \tag{8}$$

where $\sigma_1 = F_1/(L_2 \cdot b)$ and $\varepsilon_1 = \Delta x_1 / L_1$. Axial modulus $E_2^*$ can be easily obtained following the same procedure. The Shear Modulus $G_{12}^*$ represents the elastic modulus used to describe, in the plane $\{x_1, x_2\}$ the relationship between the deformation that occurs in the RVE when it is subject to a force parallel to one of its edge while its opposite edge undergoes an opposing force, as illustrated in figure 6c. It is the ratio of the shear stress $\tau$ divided by the shear strain $\gamma$. Shear stress is the force $F_2$ applied parallel to the edge with normal 1 along direction 2, divided by the cross-sectional area, $L_2 \cdot b$. The shear strain, for small deformation, can be defined as the transverse displacement $\Delta w$ divided by the initial length $L_1$.

$$G_{12}^* = \frac{\tau}{\gamma} \tag{9}$$

where $\tau = F_2/(L_2 \cdot b)$ and $\gamma = \Delta w / L_1$. Shear modulus $G_{21}^*$ can be easily obtained following the same procedure.

It is necessary to underline that while for regular patterns the RVE can be explicitly identified and statically solved to obtain the expression of $E_1^*$, $E_2^*$, $G_{12}^*$ and $G_{21}^*$ in closed form, this is not possible for the patterns derived from the Voronoi tessellation,

due to their inherent irregularity. The approach here proposed consists in defining the correlation between the mechanical properties of the irregular (Voronoi) and regular (hexagrid) patterns, the former obtained from the latter through Eqs. (6-7) for $\alpha \neq 0$. The aim is to the define appropriate correction factors $\eta_{Ei}$:

$$\eta_{Ei} = \frac{E^*_{i,V}}{E^*_{i,H}}, \eta_{Gij} = \frac{G^*_{ij,V}}{G^*_{ij,H}} \qquad (10)$$

where the subscripts H and V refer, respectively, to the regular hexagrid and the relative Voronoi diagram. The ratios $\eta_{Ei}$, $\eta_{Gij}$ allow for calculating the mechanical proprieties of the Voronoi pattern characterised by a specific value of the irregularity factor, α, starting from the ones of the "original" honeycomb pattern, characterized by the same number of seed points.

In the following, the procedure for obtaining the mechanical properties of a regular honeycomb is briefly recalled from (Montuori *et al*. 2015); subsequently, the procedure for deriving the correction factors for the Voronoi counterpart is described.

## Mechanical proprieties of the regular honeycomb

The Relative Density $\rho$ is an important scalar geometrical quantity, defined as the ratio of the volume occupied by the solid material, $\rho^*$, to the total volume of the cell, $\rho_{vol}$. For the unit cell of a 2D grid made of one dimensional beam elements (see figure 7), the definition of ρ becomes:

$$\rho = \frac{\rho^*}{\rho_{vol}} = \frac{\sum_{i=1}^{n} \ell_i A_i}{L_1 L_2 b} \qquad (11)$$

where *n* is the total number of beams in the unit cell, $\ell_i$ and $A_i$ are respectively the length and the cross section area of beams, $L_1$ and $L_2$ are respectively the dimensions of the 2D unit cell along a $x_1$ and $x_2$ directions, b is the thickness of the unit cell, i.e. the width of the beam cross section.

For a regular hexagrid, the relative density generically defined by means of Eq. 11, can be further specialised according to the following equation (figure 7):

$$\rho = \frac{(h A_h) + (2 d A_d)}{\left[(h + d\,Cos\theta)(2 d\,Sin\theta)\right] b} \qquad (12)$$

where h and d are respectively the lengths of the horizontal and diagonal beams, $A_h$ and $A_d$ are respectively the cross sectional areas of the horizontal and diagonal beams, θ is the angle between the diagonal element and the horizontal axis. Considering a regular hexagonal grid, the RVE can be easily established by looking at the deformation modes and internal force distributions arising in the unit cell as a part of the global grid, under axial and shear tests. figure 8, figure 9, figure 10 and figure 11 show the static schemes of the RVE, to be adopted for carrying out the axial and shear tests, respectively; more details can be found in (Montuori *et al*. 2015).

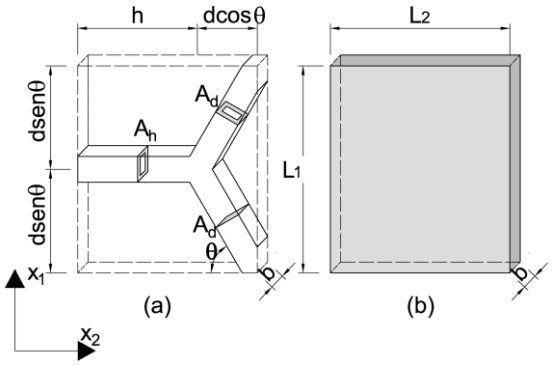


**Figure 7**. Hexagrid. Definition of the relative density for the unit cell.

For the axial test the global axial deformation of the RVE is given by the contributions of local bending, axial and shear deformations of the RVE structural members.

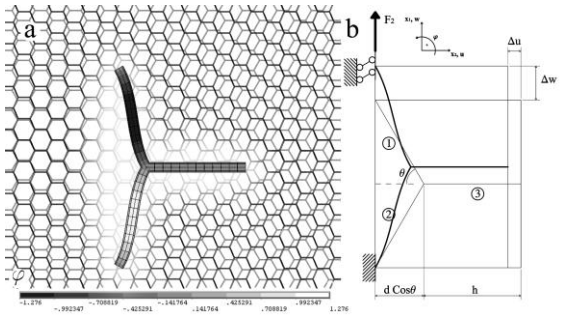


**Figure 8**. Hexagrid axial test along $x_1$; a) deformed configuration; b) definition of the RVE.

Therefore the stiffness of the hexagrid in $x_1$ direction, $E^*_{1H}$, (figure 8) normalised to the Young's modulus of the member solid material $E_s$, is given by:

$$\frac{E^*_{1,H}}{E_s} = \frac{d\,Sin\theta}{(h + d\,Cos\theta) b} \left\{ \frac{d}{A_d} Sin^2\theta + \left[ \frac{d^3}{12 I_d} + \frac{2d}{A_d} \chi_d (1+\nu) \right] Cos^2\theta \right\}^{-1} \qquad (13)$$

where $I_d$ is the inertia of the cross sectional areas of the diagonal beams respect to the flexural axis. The stiffness of the hexagrid in $x_2$ direction, $E^*_{2H}$, (figure 9), normalised to the Young's modulus of the member solid material $E_s$, is given by:

$$\frac{E^{*}_{2,H}}{E_s} = \frac{h+d\,Cos\theta}{2\,d\,Sin\theta\,b}\left[\frac{h}{A_h}+\frac{d}{2A_d}Cos^2\theta+\left[\frac{d^3}{24I_d}+\frac{d}{A_d}\chi_d(1+\nu)\right]Sin^2\theta\right]^{-1} \quad (14)$$

Considering the shear tests (figure 10 and 11), the global shear distortion of the unit cell, $\Delta w$ and $\Delta u$, is caused by shortening/lengthening of elements subjected to axial forces, by shear deformation of elements under shear forces and by flexural deflection of elements subjected to bending moments.

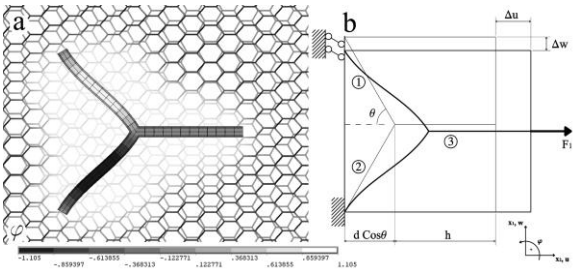


**Figure 9**. Hexagrid axial test along $x_2$; a) deformed configuration; b) definition of the RVE.

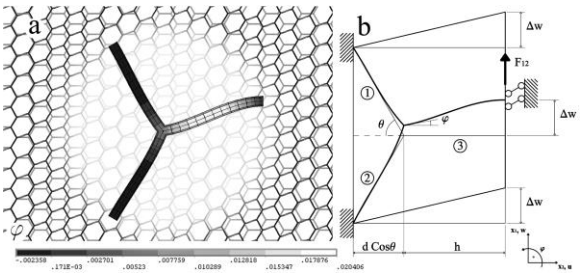


**Figure 10**. Hexagrid shear test; a) deformed configuration; b) definition of the RVE.

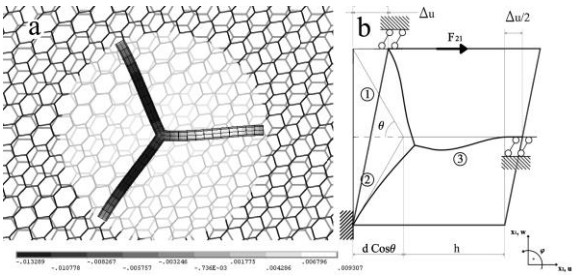


**Figure 11**. Hexagrid shear test; a) deformed configuration; b) definition of the RVE.

Therefore the shear stiffnesses of the hexagrid, $G^{*}_{12H}$ and $G^{*}_{21H}$, normalised to the shear modulus of the member solid material, $G_s$, are given by:

$$\frac{G^{*}_{12,H}}{G_s} = \frac{12I_d(1+\nu)(h+d\,Cos\theta)}{b\,d\,h^5 Sen\theta}\cdot\left\{6E_s^2\gamma_1+\frac{A_h h^5\left(1-\frac{I_h+\gamma_1\gamma_{13}}{h^3\gamma_{11}}\right)}{A_h h^2+24I_h(1+\nu)\chi_h}\right\} \quad (15)$$

$$\frac{G^{*}_{21,H}}{G_s} = \frac{4(1+\nu)Sen\,\theta}{b(h+d\,Cos\theta)\,d^5}\cdot\left\{6I_d Sen^2\theta\left[6E_s^2\gamma_3+\frac{A_d d^5\left(1+\frac{2Cos\theta\left(d\,I_d+\frac{\gamma_3\gamma_{13}}{2}\right)}{d^4\gamma_{11}}\right)}{A_d d^2+24I_d(1+\nu)\chi_d}\right]+-A_d d^5 Cos\theta\left[\frac{Sen^2\theta\left(d\,I_d+\frac{\gamma_3\gamma_{13}}{2}\right)}{d^4\gamma_{11}}-\frac{1}{2}Cos\theta\right]\right\}$$

(16)

Where $I_h$ is the inertia of the cross sectional area of the horizontal beam respect to the flexural axis and

$$\gamma_1 = \frac{I_h\left(\frac{\gamma_h}{I_h}I_d+\gamma_d+A_d d^2 Sen^2\theta\right)}{d^3\left(36E_s^2\gamma_{11}\gamma_{12}-\gamma_2\right)}$$

$$\gamma_2 = \gamma_{13}\left(\frac{\gamma_h}{2h^3 Cos\theta}+\frac{\gamma_d}{d^3}+\frac{A_d Sen^2\theta}{d}\right)$$

$$\gamma_3 = \frac{\frac{A_d d^3 I_h Cos\theta-\frac{d\,I_h\gamma_d}{Cos\theta}}{h^3}-2A_d I_d-\frac{d\,I_d\gamma_h}{h^3 Cos\theta}}{-36E_s^2\gamma_{11}\gamma_{12}+\gamma_2}$$

$$\gamma_h = \frac{12A_h h^2 I_h Cos\theta}{A_h h^2+24I_h(1+\nu)\chi_h},\quad \gamma_d = \frac{12A_d d^2 I_d Cos\theta}{A_d d^2+24I_d(1+\nu)\chi_d}$$

$$\gamma_{11} = \frac{I_h}{h^3}-\frac{2I_d Cos\theta}{d^3},\ \gamma_{12} = \frac{I_h}{h^2}-\frac{2I_d Cos\theta}{d^2}$$

$$\gamma_{13} = 2E_s^2\left(\frac{8I_d}{d}+\frac{4I_h}{h}\right)$$

The Eqs. (13-15) and Eq. (16) only contains geometrical quantities, i.e. the geometrical characteristics of the grid (θ, h, d), and the geometrical properties of the structural member cross sections ($A_h$, $A_d$, $I_h$, $I_d$, $\chi_h$, $\chi_d$ ). Therefore $E^*_{1H}/E_s$, $E^*_{2H}/E_s$, $G^*_{12H}/G_s$, and $G^*_{21H}/G_s$ represent the effective elastic properties of the reference sample (RVE), accounting for the global geometry of the grid and the local geometry of the member cross-sections.

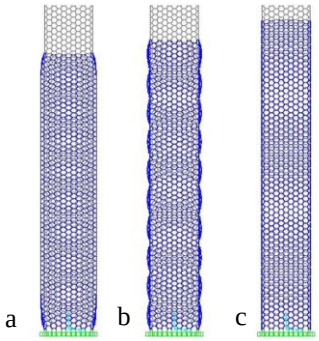


**Figure 12**. Effect of the Rigid Floor Diaphragm on Hexagrid Tubular Structures.

This theoretical approach is the one commonly adopted for 2D cellular solid, based on the definition of a representative volume element (RVE), i.e. the unit statistically representative of an infinite periodic structure. In order to assess the representativeness of the RVE defined in figure 8, 9, 10, 11 and the reliability of the Eqs. (13-15) and Eq. (16) a sensitivity analysis has been carried out: axial and shear tests have been executed on grid panels made of periodic arrangements of k RVEs along $x_1$ and $x_2$ directions, with $k \in \{1,3,5,7,10,13,15\}$. The overall stiffness values calculated from the analyses prove to be in very good agreement with the values obtained through the RVE calculations.

**Effect of the floor rigid diaphragm**

In (Montuori *et al*. 2015) the application of the Eqs. (13-15) and Eq. (16) for the design of a tall building model with tube hexagonal structure has shown some important issues; in particular, the comparison of the design values of the top horizontal displacement to the results of FEM analysis, initially showed significant discrepancies. The main source of this large scatter is related to the effect of the rigid floor diaphragm (RD), which provides an additional restraint in the axial deformation mode of the RVE, and, globally, of the structural grid; this, in turn, give rise to a significant increase of the flexural stiffness of the grid tube structure.

The effect of the rigid diaphragm is made clear by looking at figure 12, which shows the deformation of a tube structure under vertical loads with different number of RDs along elevation, i.e.: a)RD only at the top of the building; b) RD at every 9$^{th}$ level; c) RD at every floor. The comparison among the deformation modes suggests an analogy with the behaviour of laminated elastomeric bearings: the stiffening effect of RD on the vertical deformation of building structural grid is analogous to the confinement exercised by the steel interlayer shims on the lateral bulging of the rubber layers, which is accounted for through the primary shape factor $S_1$, which, in turn, strongly affects the vertical stiffness of the isolator. On the contrary, the presence of the RD constraints does not affect the shear deformation and the lateral stiffness of the structural pattern, as also occurs in the response of laminated rubber bearings.

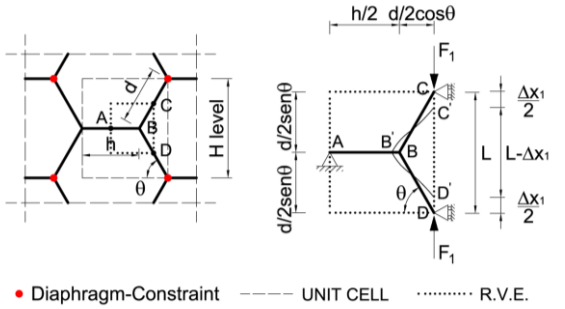


**Figure 13**. Hexagrid shear test along $x_1$: variation of the RVE due to the RD effect.

On the basis of the above considerations, two procedures have been outlined for dealing with this problem and improving the accuracy in the evaluation of the vertical stiffness modification factor: the former is based on the definition of a new, appropriate mechanical model which explicitly takes into account the RD effect (appointed as Modified RVE Approach (MRA)); the latter utilizes the analogy with Isolator deformation mode and the concept of primary shape factor (appointed as Isolator Analogy Approach (IAA)). In the following, for the sake of brevity, only the first approach is illustrated.

**Modified RVE**

The so-called Modified RVE approach, simply modifies the RVE of the hexagonal pattern (from which the Voronoi pattern is subsequently generated) in order to account for the RD additional restraint; of course, the modified RVE strongly depends on the module height, namely on the number of floors (and of RD constraints) occurring along the unit cell.

For a hexagonal patterns with height of the unit cell equal to the interstory height ($H_{unit\ cell} = H_{int}$), the RD constraint partially blocks the horizontal dilatations of the module, namely the horizontal displacements of the joints marked with solid circles in figure 13; therefore the ends of the diagonal members in the RVE cannot experience horizontal displacements and should be accordingly restrained.

The normalized vertical stiffness for the above structural model is computed through the following relationship:

$$\frac{E^*_{1,H}}{E_s} = \frac{1}{(h + d\,\mathrm{Cos}\theta)\,b} \cdot \left[ \frac{1}{A_d \mathrm{Sen}\theta} + \frac{\mathrm{Cos}^2\theta\left(\frac{d^2}{12I_d} + \frac{2\chi(1+\nu)}{A_d} - \frac{1}{A_d}\right)}{A_d \mathrm{Sen}\theta\left(\frac{d^2 \mathrm{Sen}^2\theta}{12I_d} + \frac{2\chi(1+\nu)\mathrm{Sen}^2\theta}{A_d} + \frac{\mathrm{Cos}\theta\,\mathrm{Sen}\theta}{A_d} + \frac{2}{A_h}\right)} + \frac{2h\,\mathrm{Cos}^2\theta\left(\frac{d^2}{12I_d} + \frac{2\chi(1+\nu)}{A_d} - \frac{1}{A_d}\right)}{A_h d\,\mathrm{Sen}\theta\left(\frac{d^2 \mathrm{Sen}^2\theta}{12I_d} + \frac{2\chi(1+\nu)\mathrm{Sen}^2\theta}{A_d} + \frac{\mathrm{Cos}\theta\,\mathrm{Sen}\theta}{A_d} + \frac{2}{A_h}\right)} \right]^{-1} \quad (17)$$

As already observed, the shear stiffness is not affected by the RD action, therefore the normalised shear stiffnesses are still provided by the equation (15) and (16).

In the following, for the sake of simplicity, the case $A_h = A_d = A$ and $I_h = I_d = I$ is considered, i.e. the same cross section is adopted for all the structural members of the grid. For the geometry of the grid it is assumed $h = d$ and $\theta = \pi/3$, for this case the equations (15) and (16) are identical, and therefore $G^*_{12H} = G^*_{21H}$.

## From Hexagrid to Voronoi

According to the scientific literature (Zhu *et al*. 2001) the mechanical response of the Voronoi patterns strongly depends on the level of irregularity and on the relative density. Therefore, for the definition of the correction factors which allow to characterize a Voronoi pattern starting from a regular hexagrid, it is necessary to investigate and understand the above effects.

Recalling the Eqs. (6-7), it is also evident that for a fixed number of cells of the original hexagrid, and for each values of $\alpha$ (i.e. for each level of irregularity) and of $\rho$ (i.e. for a specific relative density), infinite Voronoi configurations can be generated varying the random parameters $\varphi_s$ and $\vartheta_s$.

The RVE modeling approach used in the previous paragraph for investigating the mechanical properties of the regular honeycomb is not able to account for the irregularities in the Voronoi microstructure. In fact, the Voronoi tessellation shows a non-periodic pattern and the choice of an appropriate, statistically representative volume element is impossible due to a violation of the definition of RVE (Hole and Beckman 2012).

Since the disorder in the Voronoi structure can produce a wide range of values of the overall mechanical properties at the macroscopic level, the effect of irregularity and relative density on the mechanical proprieties of the Voronoi patterns should be assessed on a statistical basis. This is precisely the approach suggested by Hole and Beckman (2012) and adopted in the following: instead of prescribing a volume element for executing a single analysis statistically representative of the global response, a large set of repeated homogenization analyses are performed on small scale Testing Volume Elements (TVE).

For each specific couple of values of $\rho$ and $\alpha$, a set of TVE is generated varying the random variables $\varphi_s$ and $\vartheta_s$. The number of TVE herein considered is large enough to include all pattern irregularities, and, although each single TVE is not able to represent the structure at the macro scale level, the entire set of TVE can be assumed as statistically representative of the whole pattern. A critical point, therefore, is the definition of the numerosity of the TVE set; for this aim a preliminary sensitivity analysis has been carried out, as described in the following section. Furthermore through a sensitivity analysis it has been assessed that, adopting a dimension of 20X18 unit cells for the TVE, the size effect in the results of mechanical tests is negligible for the aim of this work.

The axial and shear tests have been performed through finite element (FE) analyses using the computer code SAP2000; the specimens have been modelled as assemblies of Timoshenko beam elements, which include bending, axial and shear deformations. In the FE models, the boundary conditions and the external forces reported in figure 14 have been applied in order to perform axial and shear tests.

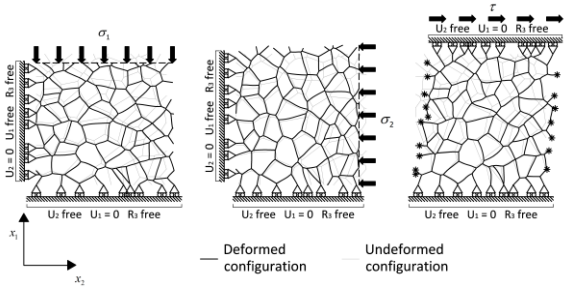


**Figure 14**. Boundary conditions and external forces adopted in the FE models of the Voronoi specimens.

Through the axial and shear tests, the values of the effective mechanical proprieties of the k-th Voronoi TVE ($E^*_{1,V,k}$, $E^*_{2,V,k}$ and $G^*_{12,V,k} = G^*_{21,V,k}$) have been obtained by homogenizing the FE numerical results, following the relationships:

$$E^*_{1,V,k} = f\left(\bar{\rho},\bar{\alpha},\varphi_s,\vartheta_s\right) \quad E^*_{2,V,k} = f\left(\bar{\rho},\bar{\alpha},\varphi_s,\vartheta_s\right)$$

$$G^*_{12,V,k} = f\left(\bar{\rho},\bar{\alpha},\varphi_s,\vartheta_s\right) \tag{18}$$

The ratio of the experimental values $E^*_{1,V,k}$, $E^*_{2,V,k}$ and $G^*_{12,V,k} = G^*_{21,V,k}$ to the original hexagrid counterparts, resulting from of Eq. (17), and Eqs. (14-15), have been computed and appointed as the modification factors $\eta_{E1,k}$, $\eta_{E1,k}$ and $\eta_{G12,k} = \eta_{G21,k}$ of axial and shear stiffness for the i-th TVE, i.e.:

$$\eta_{E1,k} = \frac{E^*_{1,V,k}}{E^*_{1,H}} \qquad \eta_{E2,k} = \frac{E^*_{2,V,k}}{E^*_{2,H}}$$

$$\eta_{G12,k} = \frac{G^*_{12,V,k}}{G^*_{12,H}} \tag{19}$$

Recalling the previous relationships, the modification factors are as well functions of $\rho$, α, $\varphi_s$ and $\vartheta_s$. In force of the probabilistic distribution of the geometrical parameters $\varphi_s$ and $\vartheta_s$, Eqs. (4-5), it is possible to assume an equal probability for the occurrence of all the analyzed TVE; then, the probability related to each TVE analysis is:

$$p\left(\eta_{E1,k}\right) = \frac{1}{N} \quad p\left(\eta_{E2,k}\right) = \frac{1}{N}$$

$$p\left(\eta_{G12,k}\right) = \frac{1}{N} \tag{20}$$

where n is the total number of numerical experiments (i.e. of TVE).

Finally the expected value for the modification factor can be calculated through the forms:

$$\eta_{E1,A}\left(\bar{\rho},\bar{\alpha}\right) = \sum_{k=1}^{n} \eta_{E1,k}\, p\left(\eta_{E1,k}\right)$$

$$\eta_{E2,A}\left(\bar{\rho},\bar{\alpha}\right) = \sum_{k=1}^{n} \eta_{E1,k}\, p\left(\eta_{E1,k}\right)$$

$$\eta_{G12,A}\left(\bar{\rho},\bar{\alpha}\right) = \sum_{k=1}^{n} \eta_{G12,k}\, p\left(\eta_{G12,k}\right) \tag{21}$$

Once defined the number n of random Voronoi specimens (TVE) to be analyzed for collecting data which can be considered statistically significant, an extensive campaign of numerical tests has been performed, varying the values of irregularity and relative density. In particular, starting from regular hexagonal patterns with the same overall geometry and number of unit cells but variable relative density ($\rho_i$ = 0.01, 0.05, 0.15, 0.20, 0.25, 0.30), n specimens have been generated for each value of irregularity (i.e. $\alpha_i$ = 0, 0.1, 0.2, 0.3, 0.4, 0.5, 0.6, 0.7, 0.8, 0.9, 1) and for each value of $\rho_i$.

An important issue that has been preliminarily addressed is the definition of the minimum number of samples to be tested, in order to have a statistical relevance of the results.

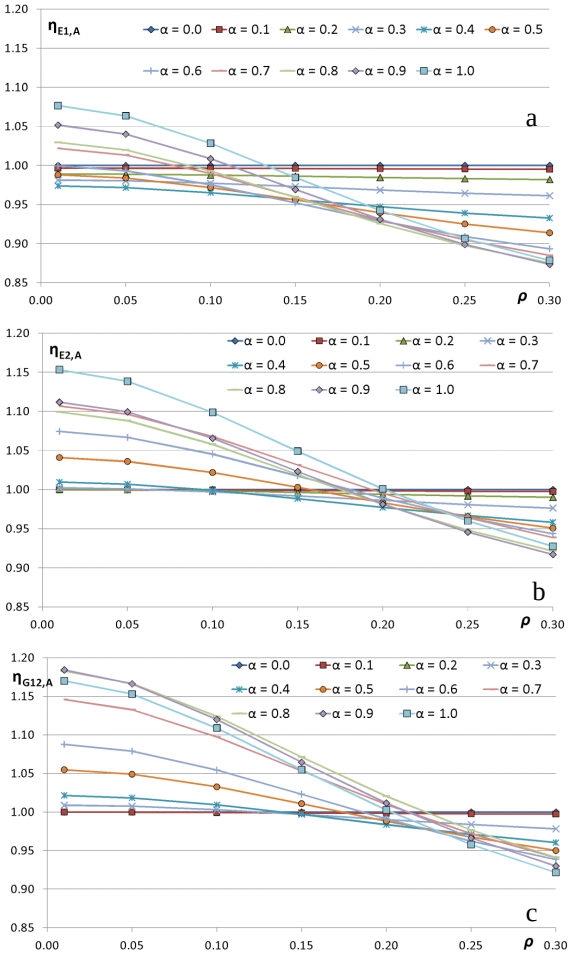


**Figure 15**. . Correction factors vs. relative density for different values of the irregularity parameter: a) $\eta_{E1,A}$; b) $\eta_{E2,A}$; c) $\eta_{G12,A}$.

Considering a "complete" irregular Voronoi pattern (α = 1) and a low relative density ($\rho$ = 0.01) the averages and the standard deviations of the mechanical properties have been calculated with different number of specimens (N = 10, 20, 30, 40, 50, 60, 70, 80). It can be observed that the standard deviation has a small variation going from 10 to 20 tests, while no change has been observed increasing the number of specimens beyond 20.

On the basis of the sensitivity analysis results, it has been possible to state that considering 20 specimens for each value of irregularity and relative density, statistically reliable results can be obtained. Recalling that 11 values of α and 6 values of $\rho$ are considered for grasping the effects of irregularity and relative density, and that for each specimen 3 numerical tests are necessary (i.e. axial tests along $x_1$ and $x_2$ directions, and shear test), then a total of 3960 analysis must be performed.

Due to the great amount of analyses to be performed, an algorithm that automates the analysis has been defined in the Grasshopper environment. In

particular the algorithm: i) exports the geometry built in grasshopper to a FE computer code (e.g. SAP2000); ii) assigns the defined cross sections to members according to the relative density $\rho$, iii) applies the external restraints and loads, iv) executes the FE analysis, v) exports the results for subsequent elaboration. Combining this algorithm with the one previously described for the generation of the Voronoi geometries, all the numerical test process is automated with a remarkable reduction of the time consumption.

## Correction Factors for Voronoi Structures

The parametric FE analysis carried out varying both relative density and irregularity provides the results reported in figure 15; the averages values ($\eta_{E1,A}$, $\eta_{E2,A}$ and $\eta_{G12,A}$) of the twenty correction factors values ($\eta_{E1,i}$, $\eta_{E2,i}$ and $\eta_{G12,i}$) obtained for each couple of values α and $\rho$ (varying $\varphi_i$ and $\vartheta_i$) are used as statistical response parameters. In particular the average values ($\eta_{E1,A}$, $\eta_{E2,A}$ and $\eta_{G12,A}$) are as a function of $\rho$ for different values of α, figure 15.

Results show that, varying α between 0.1 and 0.6, $\eta_{E1,A}$ is always smaller than 1, meaning that the axial stiffness along $x_1$ of the Voronoi pattern is lower than the one of the regular hexagonal structure; in addition, $\eta_{E1,A}$ decreases as $\rho$ increases, i.e. the Voronoi patterns are less stiff than the hexagrid counterparts as the relative density increases. For higher levels of irregularity (α > 0.7) and low densities, the figure 15a reveals that $\eta_{E1,A}$ increases and becomes greater than 1 (maximum value equal to 108% for α = 1 and $\rho$ = 0.01); however, for $\rho$ greater than 0.15, a reduction of $\eta_{E1,A}$ can be observed (minimum value equal to 88% for α = 1 and $\rho$ = 0.3). A similar trend can be observed for both $\eta_{E2,A}$ and $\eta_{G12,A}$: for low densities ($\rho$ < 0.2) the correction factors are always greater than 100%, i.e. the Voronoi specimens are always stiffer than the hexagonal counterparts, while increasing the density ($\rho \geq 0.2$) both factors $\eta_{E2,A}$ and $\eta_{G12,A}$ decrease.

It has been reported in a three dimensional coordinate system the values of $\eta_{E1,A}$, $\eta_{E2,A}$ and $\eta_{G12,A}$, respectively, as a function of α and $\rho$, and the surfaces that best fit the point distributions. The three surfaces are represented by polynomial expressions, which define $\eta_{E1,A}$, $\eta_{E2,A}$ and $\eta_{G12,A}$ as functions of α and $\rho$, i.e.:

$$\begin{aligned}\eta_{i,A} = f(\rho,\alpha) = k_{00} + k_{10}\cdot\alpha + k_{01}\cdot\rho + k_{20}\cdot\alpha^2 + \\ + k_{11}\cdot\alpha\cdot\rho + k_{02}\cdot\rho^2 + k_{30}\cdot\alpha^3 + k_{21}\cdot\alpha^2\cdot\rho + \\ + k_{12}\cdot\alpha\cdot\rho^2 + k_{03}\cdot\rho^3 + k_{31}\cdot\alpha^3\cdot\rho + k_{22}\cdot\alpha^2\cdot\rho^2 + \\ + k_{13}\cdot\alpha\cdot\rho^3 + k_{04}\cdot\rho^4\end{aligned} \quad (22)$$

The polynomial coefficients ($k_{ij}$) for each surface $\eta_{E1,A}$, $\eta_{E2,A}$ and $\eta_{G12,A}$ are reported in tab. 1

**Table 1.** Polynomial coefficients ($k_{ij}$) for the values of $\eta_{E1,A}$, $\eta_{E2,A}$ and $\eta_{G12,A}$

| | $k_{00}$ | $k_{10}$ | $k_{01}$ | $k_{20}$ | $k_{11}$ | $k_{02}$ | $k_{30}$ |
|---|---|---|---|---|---|---|---|
| $\eta_{E1,A}$ | 1,0053 | -0,1780 | -0,0049 | 0,3271 | 1,0999 | -0,6239 | -0,0758 |
| $\eta_{E2,A}$ | 1,0040 | -0,1634 | -0,0018 | 0,6516 | 1,2630 | -0,7284 | -0,3474 |
| $\eta_{G12,A}$ | 1,0130 | -0,3878 | -0,0135 | 1,4150 | 2,0090 | -1,0260 | -0,8586 |
| | $k_{21}$ | $k_{12}$ | $k_{03}$ | $k_{31}$ | $k_{22}$ | $k_{13}$ | $k_{04}$ |
| $\eta_{E1,A}$ | -2,5603 | -5,4090 | 5,0768 | 1,3993 | 0,2842 | 10,5875 | -10,2391 |
| $\eta_{E2,A}$ | -3,0570 | -6,2510 | 5,7720 | 1,7380 | 0,5064 | 11,7500 | -11,4600 |
| $\eta_{G12,A}$ | -5,1820 | -7,3450 | 7,6560 | 3,1010 | 0,7922 | -13,6000 | -14,9000 |

## Design procedure

The design procedure delineated in paragraph 2 can be now applied, and the Eq. (3) can be rewritten as:

$$\delta_{tot} = \delta_{bending} + \delta_{shear} = \frac{q\,H^4}{8\cdot E^*_{1,H}\,\eta_{E1,A}\,I} + \frac{q\,H^2}{2\cdot G^*_{12,H}\,\eta_{G12,A}\,A}\chi = \frac{H}{500} \quad (23)$$

where: $E^*_{1,H}$ and $G^*_{12,H}$ can be expressed using the Eqs. (15-16) respectively; $\eta_{E1,A}$ and $\eta_{G12,A}$ are only function of the relative density through Eq. (22), fixed the irregularity degree of the Voronoi patterns (i.e. the value of α).

Given the overall dimensions of the building (I, A and H) and the external forces (q), in the Eq. (23) the only unknown values are the geometrical properties of the structural members of the Voronoi grid, which appear in Eq. (17), and Eqs. (14-15).

The dimensions of the structural elements of the Voronoi grid obtained solving Eq. (23), allow to satisfy the stiffness requirements, i.e. to have a top drift of the building less than H/500. It is worth noticing that the Eq. (23) cannot be solved in closed form, due to the high complexity of the equations in play, therefore a numerical solution is necessary.

In order to assess the accuracy of the design procedure and of the formulations proposed in this paper, a real application to a building model has been developed.

The building model utilised for the design applications is characterized by plan dimensions and height equal to the Sinosteel International Plaza (Fu *et al.* 2012), i.e.: height 351 m, 90 stories, interstory height 3.9 m, square plan dimension 53x53 m. A horizontal wind action, modelled as a uniform load of 200 kN/m, has been considered in the application of the stiffness design criterion.

The structure has a central core with a simple frame that carries only the gravity loads and does not provide any contribution under horizontal loads. On the building perimeter a Voronoi pattern of structural members has been generated, giving rise to a Voronoi tube structure which carries tributary gravity loads and total wind loads (figure 16). The Voronoi pattern is generated starting from a regular hexagonal pattern, with ten hexagonal cells along each plan direction,

and applying the maximum level of irregularity (i.e. $\alpha = 1$) to the hexagonal configuration.

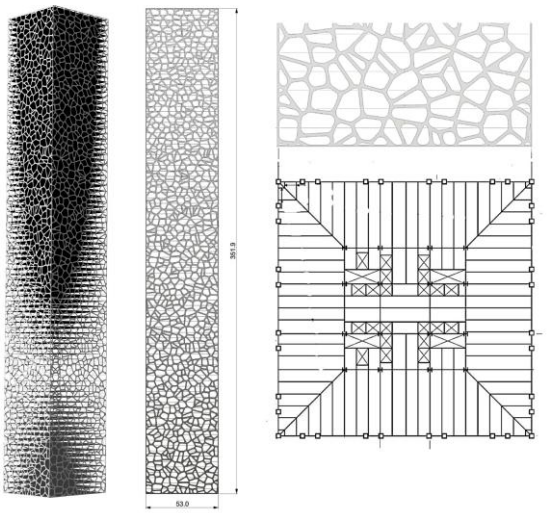

**Figure 16**. Voronoi building, plan and elevation.

The cross section area of the Voronoi grid members can be calculated by means of Eq. (23); fixing the thickness of the cross section of the Voronoi grid, the overall geometrical properties of the building are known. Numerically solving the Eq. (23), square section 1100x1100 have been obtained.

The performance of the Voronoi structure designed according to the proposed procedure has been checked by means of finite element analysis, using the computer code SAP2000. The structures is modelled as an assemblage of Timoshenko beams, which include bending, axial and shear deformations; at the building base, the joints are fixed and rigid diaphragms constraints are assigned to the nodes of each floor. The wind load is modelled as concentrated forces applied at the centre of gravity of each floor.

The horizontal displacements and the interstory drift along the building height are reported in figure 17a and b, respectively; it is worth noticing that both the top displacement of the building and the interstory drift are less than the design limits (i.e. H/500 and h/200 respectively), thus confirming the efficacy of the design procedure proposed in the paper.

Possible improvements, concerning member size optimization as well as density and/or regularity variations along the buildings height (figure 18) can be easily obtained through the proposed approach.

## Conclusions and further developments

This paper has considered non regular patterns based on Voronoi diagrams as structural grid for tall building façades; after having discussed the procedure for the generation of Voronoi diagrams, the authors have defined a methodology for the mechanical characterization and the homogenization process of a Voronoi structural grid, which has also been specified with reference to the case of tall buildings facades; finally a design procedure is proposed, applied to and validated for a model building.

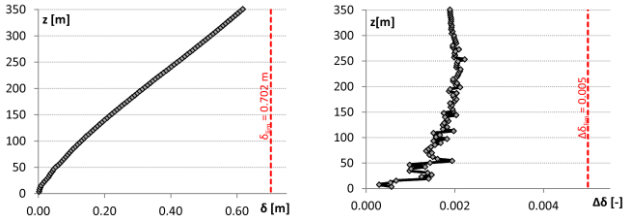


**Figure 17**. Voronoi building displacement (a), and interstory drifts under horizontal loads (b).

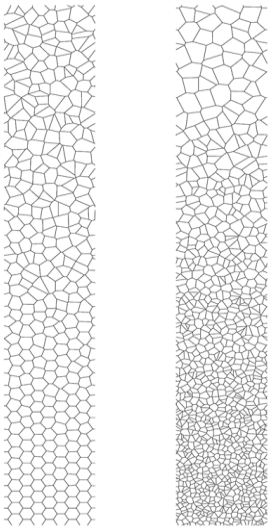

**Figure 18**. Possible improvements of Voronoi structures.

The paper makes use of an approach based on the definition and mechanical assessment of the RVE, starting from which the homogenization of the building façades is carried out; then a global stiffness design method is applied to the homogeneous cantilever beam equivalent to the tall building and the procedure for deriving the peculiar aspects related to the building scale and behaviour, such as the presence of rigid floor diaphragm, are explicitly accounted for, reflecting in a non-negligible stiffening effect on the grid global behaviour.

The design procedure which has been tested against the FE analysis of a building model seems particularly useful for the preliminary design; in fact, it allows for defining the cross sections of a very large number of structural members, assembled according to an apparently random grid, by means of simple relationships. Of course structural analysis of the discrete structural grid is still necessary in the

phase of refined design and optimization. However the authors stress the usefulness of a straightforward tool for the initial sizing phase of a non conventional structural pattern.

The study presented in this paper is part of a wide research, aimed to explore the non-conventional, bio-inspired patterns, alternative to the diagrid, to be used as façade structural grids for tall buildings. In this paper the theoretical background for providing a common methodology in dealing with non-conventional patterns for tube-like structures has been presented; further, the method has also been translated into a simplified tools for preliminary design and structural member sizing.

Within the framework of the proposal approach, it is possible to deal with geometrical patterns characterized by density and/or irregularity degree variable along the building height. Finally, member size optimization, best tuning the strength and stiffness along the elevation, can be obtained with small effort and retaining the conceptual consistency of the procedure.

In the author's opinion, a worthy aspect of novelty of the research is the definition of a framework which embraces an almost endless variety of structural configurations, going from the traditional square/rectangular frame, to the diagrid, hexagrid, Voronoi, foam/bubbles trusses, and beyond. Moreover, absolutely novel is the transfer of a methodological approach typical of the material science and engineering disciplines to the context of structural engineering, particularly the structural engineering of tall buildings. Therefore the research constitutes an example of cross-fertilization between science and architecture/engineering, which goes well beyond the nature-inspired forms of contemporary architecture, since it provide a repertoire of objects (patterned structural solutions) and the tools for dealing with them.

## References


Aurenhammer, F. (1991) Voronoi Diagrams — A Survey of a Fundamental Geometric Data Structure. *ACM Computing Surveys (CSUR)*, Vol. 23 (3), pp. 345-405.

Baker, W. F. (2013) *The Tall Buildings Reference Book*. New York, Routledge.

Beghini, L. L., Beghini, A., Katz, N., Baker, W. F., Paulino, G. H (2014). Connecting architecture and engineering through structural topology optimization. *Eng Struct*, Vol. 59, pp. 716–726.

Bock, M., Tyagi, A.K., Kreft, J.U.. Alt W. (2010) Generalized Voronoi tessellation as a model of two- dimensional cell tissue dynamics. *Bull Math Biol*, Vol. 72, pp. 1696-1731.

Burry, J., Burry, M. (2010) *The New Mathematics of Architecture*. New York, Thames & Hudson.

deMeijer, J. H. M. (2012) Lateral stiffness of hexagrid structures. *Master's thesis, University of Technology Department of the Built Environment Structural Design, Eindhoven*.

eVolo (2010). A City Within a Skyscraper for Battery Park. From: http://www.evolo.us/architecture/a-city-within-a-skyscraper-for-battery-park.

Fazekas, A., Dendievel, R., Salvo, L., Bréchet, Y. (2002) Effect of microstructural topology upon the stiffness and strength of 2d cellular structures. *Int J Mech Sci*, Vol. 44, pp. 2047-2066.

Fraldi, M., Cowin, S. (2004) Inhomogeneous elastostatic problem solutions constructed from stress-associated homogeneous solutions. *J Mech Phys Solids*, Vol. 52, pp. 2207-2233.

Fu, X.Y., Gao, Y., Zhou, Y., Yang, X. (2012) Structural Design of Sino Steel International Plaza. *CTBUH 2012 9thWorld Congress*, Shanghai.

Gibson, L.J., Ashby, M,F. (1997) *Cellular Solids: structure and properties (2nd Ed.)*. Cambridge, Cambridge University Press. .

Hashin, Z., Shtrikman, S. (1996) A variational approach to the theory of elastic behaviour of multiphasematerials. *J Mech Phys Solid*, Vol. 11, pp. 127–140.

Hensel, M., Menges, A., Weinstock, M. (2009) Emergence: Morphogenetic Design Strategies. *Architectural Design*, London, Wiley.

Hohe, J., Beckman, C. (2012) Probabilistic homogenization of hexagonal honeycombs with perturbed microstructure. *Mech Mater*, Vol. 49, pp. 13-29.

Kwan, A. K. H. (1994). Simple method for approximate analysis of framed tube structures. *J Struct Eng*, Vol. 120 (4), pp.121-1239.

Lakes, R., Materials with structural hierachy. *Nature*, Vol. 361, pp. 511-515.

LAVA (2007). Bionic Tower. From: http://www.l-a-v-a.net/projects/bionic-tower/.

Li, K., Gao, X. L., Roy, A. (2003) Micromechanics model for three-dimensional open-cell foams using a etrakaidecahedral unit cell and Castigliano's second theorem. *Compos Sci and Technol*, Vol. 63, pp. 1769-1781.

Li, K., Gao, X. L., Subhash, G. (2005) Effects of cell shape and cell wall thickness variations on the elastic properties of two-dimensional cellular solids. *Int J Solids Struct*, Vol. 42, pp. 1777-1795.

Mele, E., Toreno, M., Brandonisio, G., De Luca, A. (2014) Diagrid structures for tall buildings: case studies and design considerations. *Struct Des Tall Spec*, Vol. 23, pp. 124–145.

Montuori, G.M., Mele, E., Brandonisio, G., De Luca, A. (2013) Design criteria for diagrid tall

buildings: Stiffness versus strength. *Struct Des Tall Spec*, Vol. 23, pp. 1294-1314.

Montuori, G.M., Mele, E., Brandonisio, G., De Luca, A. (2014a) Geometrical patterns for diagrid buildings: Exploring alternative design strategies from the structural point of view. *Eng Struct*, Vol. 71, pp. 112–127.

Montuori, G.M., Mele, E., Brandonisio, G., De Luca, A. (2014b) Secondary bracing systems for diagrid structures in tall buildings. *Eng Struct*, Vol. 75, pp. 477–488. .

Montuori, G.M., Fadda, M., Perrella, G., Mele, E. (2015) Hexagrid – hexagonal tube structures for tall buildings: patterns, modeling, and design. *Struct Des Tall Spec*, Vol. 24, pp. 912-940.

Nemat-Nasser, S., Hori, M. (1999) *Micromechanics: Overall Properties of Heterogeneous Materials (2nd Ed.)*. Amsterdam, North-Holland.

Perez, G.A., Gomez, M.F. (2009) Natural structures: strategies for geometric and morphological optimization. *Proceedings of the International Association for Shell and Spatial Structures (IASS) Symposium*, Valencia.

Silva, M. J., Gibson, L. J., Hayes, W. C. (1995) The effects of non-periodic microstructure on the elastic proprieties of two-dimensional cellular solids. *Int J Mech Sci*, Vol. 37, pp. 1161-77.

Silva, M.J., Gibson, L.J. (1997). The effects of non-periodic microstructure and defects on the compressive strength of twodimensional cellular solids. *Int J Mech Sci*, Vol. 39, pp. 549–563. .

Vajjhala, S., Kraynik, A. M., Gibson, L. J. (2000) A cellular solid model for modulus reduction due to resorption of trabeculae in bone. *J Biomech Eng-T ASME*, Vol. 122, pp. 511–515.

Voronoi, G. (1908) Nouvelles applications des paramètres continus à la théorie des formes quadratiques. *Journal für die Reine und Angewandte Mathematik* , Vol. 133, pp. 97–178.

Wigner, E., Seitz, F. (19923) On the constitution of metallic sodium. *Phys Re*, Vol. 43, pp. 804-810.

Zheng, Z., Yu, I., Li, J. (2005) Dynamic crushing of 2D cellular structures: A finite element study. *Int J Impact Eng*, Vol. 32, pp. 650-664.

Zhu, H. X., Hobdell, J. R., Windle, A. H. (2001) Effects of cell irregularity on the elastic properties of 2D Voronoi honeycombs. *J Mech Phys Solids*, Vol. 49, pp. 857-870